Improved Carrier Tunneling and Recombination in Tandem Solar Cell with p-type Nanocrystalline Si Intermediate Layer

Jinjoo Park[1] · Sangho Kim[2] · Pham duy Phong[3] · Sunwha Lee[3] · Junsin Yi[3]*

[1]Major of energy and appllied chemistry, Division of Energy & Optical Technology Convergence, Cheongju University, Cheongju 28503, Korea
[2]Department of Energy Science, Sungkyunkwan University, Suwon 16419, Korea
[3]College of Information and Communication Engineering, Sungkyunkwan University, Suwon 16419, Korea

ABSTRACT: The power conversion efficiency (PCE) of a two-terminal tandem solar cell depends upon the tunnel-recombination junction (TRJ) between the top and bottom sub-cells. An optimized TRJ in a tandem cell helps improve its open-circuit voltage (V_{oc}), short-circuit current density (J_{sc}), fill factor (FF), and efficiency (PCE). One of the parameters that affect the TRJ is the buffer layer thickness. Therefore, we investigated various TRJs by varying the thickness of the buffer or intermediate layer (TRJ-buffer) in between the highly doped p-type and n-type layers of the TRJ. The TRJ-buffer layer was p-type nc-Si:H, with a doping of 0.06%, an activation energy (E_a) of 43 meV, an optical gap (E_g) of 2.04 eV, and its thickness was varied from 0 nm to 125 nm. The tandem solar cells we investigated were a combination of a heterojunction with intrinsic thin layer (HIT) bottom sub-cell and an a-Si:H (amorphous silicon) top sub-cell. The initial cell efficiency without the TRJ buffer was 7.65% while with an optimized buffer layer, its efficiency improved to 11.74%, i.e., an improvement in efficiency by a factor of 1.53.

Key words: Tandem solar cell, Tunnel recombination junction, Buffer layer, Amorphous silicon

1. Introduction

Tunnel-recombination junction (TRJ) is a significant component in a silicon-based tandem solar cell[1-10] as well as in organic solar cells[11]. Various investigations show that an optimized p/n junction is necessary to improve the performance of the tandem cell. Charge carriers from the two-neighboring sub-cells should recombine in the TRJ. However, when the TRJ structure is not optimized, a tandem solar cell may show a poor current−voltage (I−V) characteristic curve. One of the primary reasons could be the sharp band bending at the p/n interface that prevents the electron−hole transfer across the junction. Such a sharp band bending can be modified by a suitable buffer layer, as is investigated here.

Therefore, one of the basic requirements to obtain a high efficiency tandem solar cell is an optimized TRJ. The TRJ should be formed at the interface between the two cells, where doped p-type and n-type layers of two sub-cells meet. In a p−i−n-type top cell, this junction is formed by the n-type layer of the top sub-cell and the p-type layer of the bottom one. As per

quantum mechanical principle, the tunneling across a barrier depends on the barrier height and its width; a lower barrier height and a thinner barrier can show higher tunneling. Furthermore, not only tunneling but also a recombination of the charge carriers is required. A defective interlayer can enhance such a recombination[1,6,12]. However, the total recombination can decrease with a thinner interlayer. Therefore, an optimized TRJ also involves an optimized interlayer thickness. In our investigation, we observed the optimization by estimating the variation in the device characteristics when TRJ thickness was varied; in an optimized device, its efficiency is the highest. Various interlayers were investigated for the TRJ; for example, a p-type microcrystalline silicon layer[4], p+ a-Si:H layer[8,13], n-type micro-crystalline silicon[14], microcrystalline silicon oxide layer[15,16], microcrystalline n−i−p junction[4,5,17], and organic thin film[11]. These investigations further indicate the need for an optimized TRJ in a tandem solar cell.

Silicon tandem solar cell contains amorphous or nanocrystalline silicon layers. The amorphous and nanocrystalline silicon layers are popular components in a tandem cell and also popular for the TRJ formation. A thin a-Si:H layer can act as a passivator, separator or recombination center. In a tandem cell,

*Corresponding author: junsin@skku.edu

the efficient recombination of the electron−holes from the neighboring cells to the TRJ is necessary. A defective thin a-Si:H layer at the TRJ can enhance the carrier recombination thereby improving the device efficiency. Several investigations suggest that such a thin a-Si:H layer can efficiently recombine the carriers. In our investigation, we observed the optimization by estimating the variation in device characteristics when the TRJ was varied. Therefore, in an optimized device, the expected efficiency of the device is the highest.

2. Experimental Details

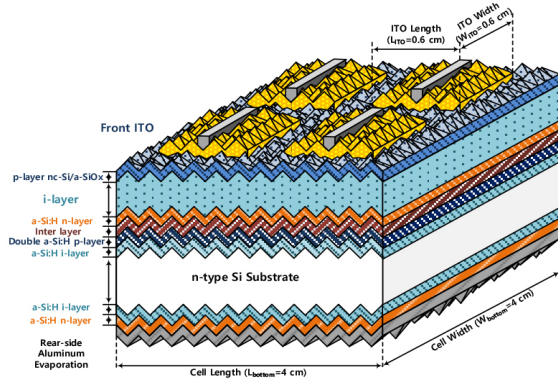We used an a-Si:H/HIT-type tandem cell structure: The top cell was the amorphous silicon type while the bottom cell was a c-Si-based heterojunction with a thin intrinsic amorphous silicon passivation layer, or a HIT cell. The amorphous or nano-crystalline layers were deposited at 13.56 MHz radio-frequency (RF) plasma-enhanced chemical vapor deposition (RF-PECVD), while transparent conducting oxide (TCO) electrodes were deposited by RF magnetron sputtering. Ag/Al metal electrodes were deposited by thermal evaporation. A schematic diagram of the tandem solar cell is shown in Fig. 1.

The source gases used in the PECVD system were silane (SiH_4), germane (GeH_4), carbon dioxide (CO_2), hydrogen (H_2), phosphine (PH_3), and diborane (B_2H_6). Different layers were deposited using different deposition conditions and source gases. A brief summary of the deposition conditions for all the layers are listed in Table 1.

Between the two sub-cells of the tandem cell, the HIT-type bottom sub-cell was prepared first, using c-Si wafers. At the front (polished) side of the wafers, the a-Si:H(i) passivation layer and a-Si:H(p1, p2) emitter layers were deposited. Subsequently, the a-Si:H(i) and a-Si:H(n+) layers were deposited at the back side of the wafers. Among the set of bottom sub-cells we investigated, the deposition conditions of the a-Si:H(i/n+) were kept unchanged, while the gas phase doping ratio and hydrogen dilution ration of the emitter bi-layer (a-Si:H(p/p+) were altered to enhance the quality of the emitter. Subsequently, the cell was dipped into 1% hydrofluoric acid for 60 s to remove the native oxide to improve the interface properties. Next, an additional p-type nc-Si:H layer, as a tunnel-recombination buffer (TRJ-buffer) layer, was optimized to improve the TRJ

Fig. 1. Schematic diagram of Si-based tandem junction solar cell with the buffer layer. TRJ-buffer layer is indicated as "interlayer"

Table 1. Deposition conditions of Si-based tandem junction solar cell

Layer		Temp. (°C)	Power (W)	Gap (mm)	Press. (mTorr)	Gas flow (sccm)						Thickness (nm)
						SiH4	H2	GeH4	CO2	PH3	B2H6	
HIT Bottom cell	n₂	200	280	20	3000	33	1000			6.7/100		140
	n1	200	130	20	3000	33	3000			18.3/100		20
	i	200	50	20	1500	60	480					5
	c-Si (n-type)											
	i	200	50	20	1500	60	480					5
	p1	200	250	12	5000	30	2700				6.4/100	5
	p2	200	250	12	5000	40	1600				33.3/100	3
TRJ-Buffer	p-type nc-Si:H	180	300	20	1500	5	800				0.3/100	75
a-Si:H Top cell	n	180	50	40	200	30	120			30/100		40
	n/i buffer	180	20	20	400	10	40					10
	i	180	25	25	300	5	20	5				200
	i	180	25	25	300	5	20	7				200
	i	180	25	25	300	5	20	9				200
	i/p buffer	180	20	20	400	10	40					20
	p1	180	20	20	1500	5	500		10		1.5/100	10
	p2	180	300	20	1500	5	800				0.3/100	25

with the n-type layer of the top cell. Subsequently, n-type a-Si:H, n/i buffer, i-type SiGe:H, i/p buffer p-type a-SiOx:H, and p-type nc-Si:H layers were deposited in this order.

An indium tin oxide (ITO) film of 200±5 nm thickness was then deposited by RF magnetron sputtering, followed by the thermal evaporation of aluminum as finger-electrodes at the front side of the cells, and silver electrode was deposited on the entire rear surface for back contact. The area of the solar cell was 0.36 cm^2, determined by 6 mm × 6 mm shadow masks that was used in determining the surface area of the deposited layers. Subsequently, a suitably optimized MgF$_2$ anti-reflection coating (ARC) layer was deposited at the front surface of the cells. In our present investigation, we used textured Si wafer and varied the TRJ-buffer of the tandem cell structure. The solar cell current density−voltage (J−V) characteristics were measured under AM1.5G insolation, and the external quantum efficiency (EQE) was measured using the QEX7 (PV Measurements, Inc.)

The complete structure of the tandem cell is given below, starting from the top (sun-facing) layer: MgF$_2$/(Ag/Algrid)/ ITO/ p2-nc-Si:H/p1-a-SiO:H/i-a-Si:(buffer)/i-SiGe:Hgrading(GeH$_4$ =0.9,0.7,0.5)/n-a-Si:H(buffer)/n-nc-Si:H/p-nc-S:Hi(buffer-TRJ,75nm)/p2-a-Si:H/p1-nc-Si:H/i-a-Si:H/c-Si(n-type)/i-a-Si:H/ n1(n+)-a-Si:H/n-a-Si:H/Al.

3. Results and Discussion

3.1 TRJ−buffer

The TRJ-buffer was a p-type nc-Si:H (p-nc-Si:H) prepared with 0.06% B$_2$H$_6$ doping and high hydrogen dilution, i.e., a 1:160 ratio of SiH$_4$ to H$_2$. The composition of this layer was kept unchanged but we varied its thickness from 50 nm to 125 nm. To improve the TRJ, a boron-doped nanocrystalline thin-film silicon (p-type nc-Si:H) was used as an interlayer between the two sub-cells. In the top sub-cell, an a-Si:H (E$_g$ of 1.8 eV) was used as the absorption layer or active layer.

The basic theory of p/n junction tunneling was developed by Keldysh and Kane[11,12] and the tunneling current density can be expressed as follows:

$$J = A \exp(-BE_b^{3/2}/E_f)(\overline{E}/2)D \qquad (1)$$
$$= A \exp(-BE_b^{1/2}qW)(\overline{E}/2)D,$$

where $A = \dfrac{qm^*}{2\pi^2\hbar^3}$, $B = \dfrac{q(m^*)^{1/2}}{2^{3/2}q\hbar}$,

$$\overline{E} = \frac{2^{5/2}q\hbar E_f}{3\pi(m^*)^{1/2}E_b^{1/2}} = \frac{2^{5/2}\hbar E_b^{1/2}}{3\pi(m^*)^{1/2}W},$$
$$qE_f W = E_b$$

Additionally,

$$D = \int \left[F_c(E) - F_v(E) \times \left[1 - \exp\left(-\frac{2E_s}{\overline{E}}\right) \right] \right] dE$$

In these equations, m^* is the tunneling effective mass, W is the tunneling barrier width, E_f is the electric field in the tunneling region, E_b is the tunneling barrier height (equals E_g for simple case), $F_C(E)$ and $F_V(E)$ are the Fermi−Dirac functions for the conduction and valence bands, respectively, and $E_S = $ min (E_1, E_2) with E_1 and E_2 the energies measured from the band edges. An important assumption in the derivation of equation (1) is that the electric field is constant in the tunneling region and that the electron kinetic energy varies in a quadratic manner within the tunneling region. This equation shows that the current density across the tunnel junction depends upon the width of the tunneling barrier, W.

By increasing the boron (B) doping in the thin-film silicon, its optical bandgap (E$_g$) and activation energy (E$_a$) decreased. We have also observed that the variations in E$_g$ and E$_a$ are larger for the B-doped a-Si:H than that with the phosphorus (P) doping. Therefore, the p-type nc-Si:H was considered as a better buffer layer or intermediate layer in the p/n tunnel junction of the tandem solar cell. Furthermore, the investigations reported earlier also indicated that a p-type interlayer can be a better option to reduce the resistance of the p/n junction[2]. The n-type a-Si:H layer of the top sub-cell had an E$_a$ of 0.2 eV and an E$_g$ of 1.81 eV. The p-type a-Si:H layer of the bottom sub-cell had an E$_a$ of 0.49 eV and an E$_g$ of 1.75 eV. Of particular importance is the p-type nc-Si:H intermediate layer or TRJ-buffer layer that had a very low E$_a$ of 0.043 eV, with a higher E$_g$, the two-terminal Si-based tandem junction solar cell displayed a V$_{oc}$ of 1.56 V, J$_{sc}$ of 9.42 mA/cm^2, FF of 52.02%, and η of 7.65%, a trend that is similar to that of reference[2]. One of the reasons for the low FF and V$_{oc}$ was the poor interface properties owing to the high E$_a$ of the p-type a-Si:H for the bottom HIT sub-cell. As the p-type nc-Si:H interlayer was inserted, the recombination of carriers became easier. Fig. 2 shows the two band structures of the interface region on the two-terminal Si-based tandem junction solar cell (a) without, and (b) with the p-type nc-Si:H interlayer.
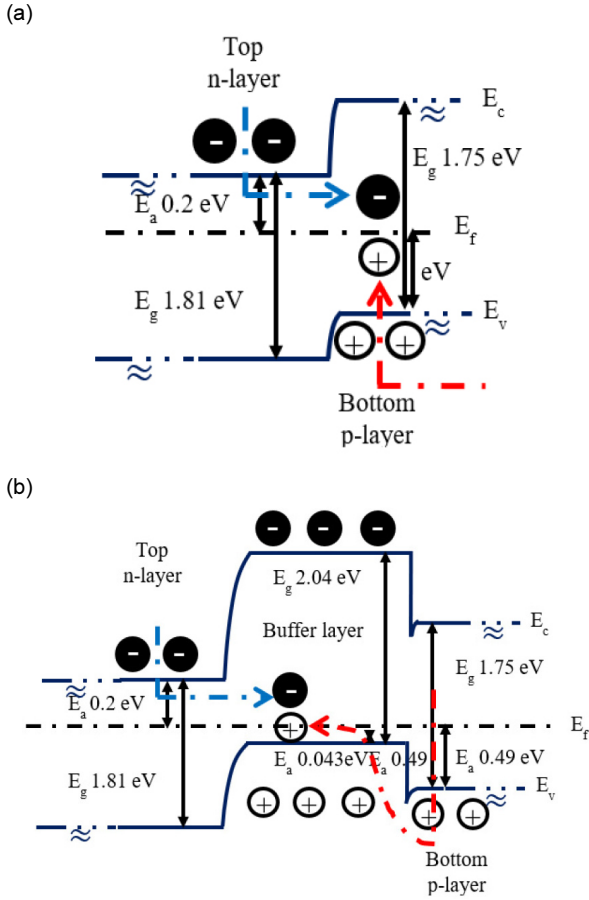
(a)

(b)

Fig. 2. Schematic band diagram of interface region on 2.04 eV. Without the p-type nc-Si:H inter layer two-terminal Si-based tandem junction solar cell (a) without, and (b) with the p-type nc-Si:H inter layer

The characteristics of the E_g and the E_a shown in Fig. 2 are shown in detail in Fig. 3. The E_g of the layers have been determined with the help of Tauc's relation[18],

$$(\alpha h\upsilon)^{1/2} = A(h\upsilon - E_g) \qquad (2)$$

where h is Plank's constant, is optical frequency, A is a constant. Optical absorption coefficient of the films, measured with the help of spectroscopic ellipsometry (SE), and $(\alpha h\upsilon)^{1/2}$ is plotted with $h\upsilon$. A linear fit is drawn at the absorption edge region and the intercept of the linear fit is used as a measure of E_g. The E_a is obtained from the temperature dependent dark conductivity $\sigma_d(T)$ by the Arrhenius relation[19],

$$\sigma_d(T) = \sigma_o \exp(-E_a/kT) \qquad (3)$$

where σ_o is a conductivity prefactor, T is the absolute temperature, and k is Boltzmann's constant.
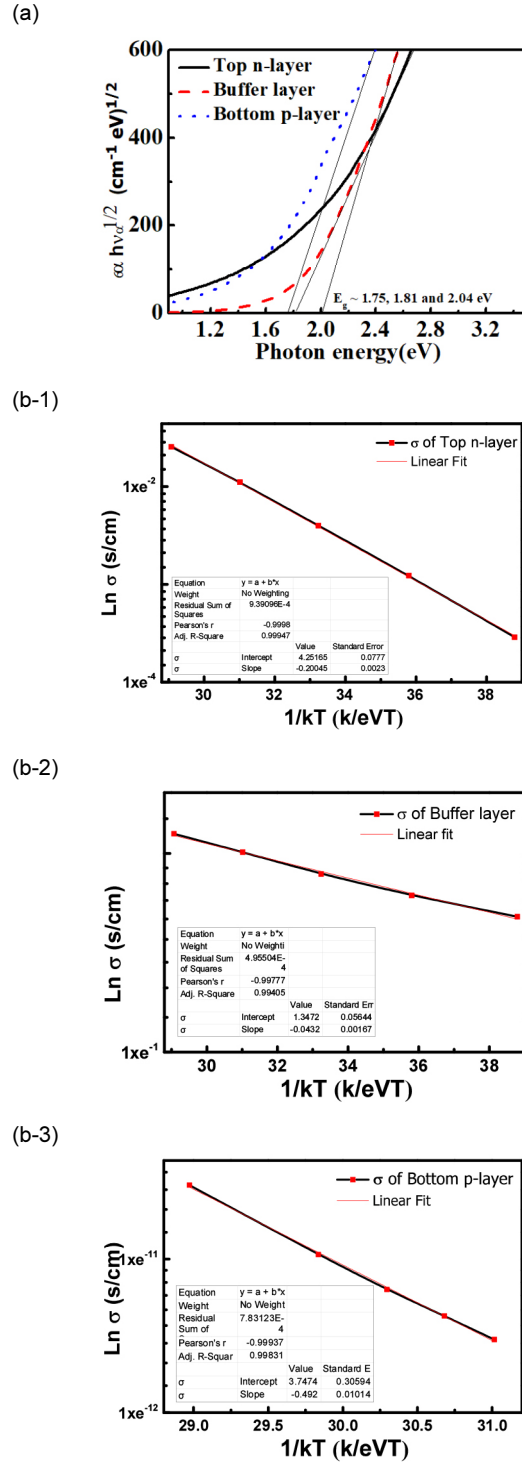
(a)

(b-1)

(b-2)

(b-3)

Fig. 3. The (a) E_g (Tauc-plot) and (b-1, b-2, and b-3) E_a (Arrhenius plot) properties for the n-type a-Si:H layer of the top sub-cell, p-type nc-Si:H buffer layer and the p-type a-Si:H layer of the bottom sub-cell

3.2 Cell fabrications

Fig. 4. shows (a) the I–V characteristic curves measured at room temperature under AM 1.5 G condition, and (b) the external quantum efficiency of the two-terminal Si-based
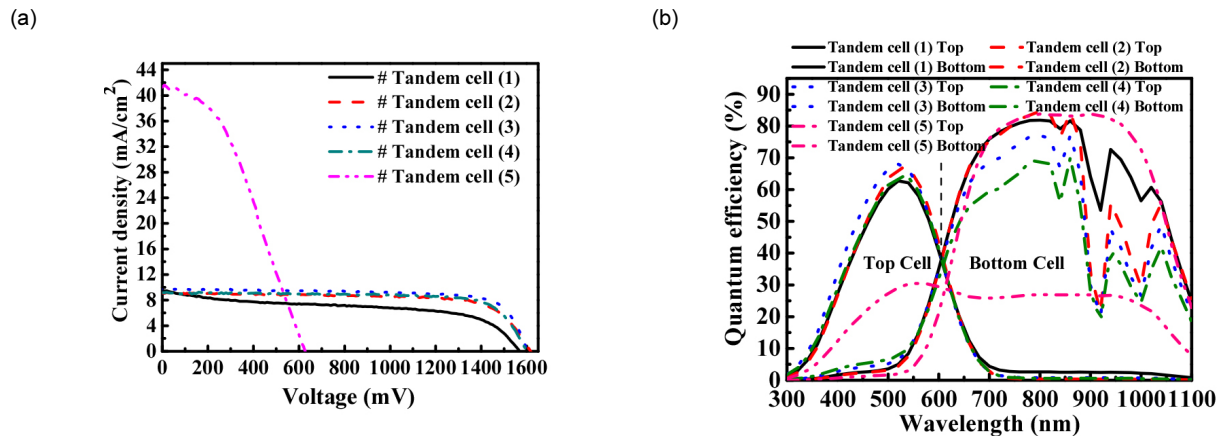
(a)

(b)

Fig. 4. (a) I−V characteristic curves measured at room temperature under A.M 1.5 G condition, and (b) external quantum efficiency of the two-terminal Si-based tandem junction solar cells with different thicknesses of the p-type nc-Si:H interlayer

Table 2. Solar cell parameters calculated by I−V characteristics curve of the two-terminal Si-based tandem junction solar cell with different thicknesses of the interlayer

Cell No.	TRJ−buffer	V_{oc} (V)	J_{sc} (mA/cm^2)	FF (%)	Eff. (%)
#1	without buffer layer	1.56	9.42	52.02	7.65
#2	with buffer layer 50 nm	1.61	9.27	73.52	10.97
#3	with buffer layer 75 nm	1.60	9.63	76.23	11.74
#4	with buffer layer 100 nm	1.59	9.15	76.65	11.15
#5	with buffer layer 125 nm	0.62	41.63	38.81	10.01

tandem junction solar cells with different thicknesses of the p-type nc-Si:H interlayer. Owing to the variation in thickness of the TRJ-buffer layer, the performance characteristics of the devices varied significantly. These parameters listed in Table 2.

Cell #5 did not have an effective tunnel junction owing to the larger thickness of the p-type nc-Si:H interlayer. The thickness of the TRJ-buffer layer was closely related with the tunneling width, *W*. Therefore, an optimum thickness of the p-type nc-Si:H inter layer, which was 75 nm, existed in our devices. The current density−voltage (J−V) characteristic curves of the solar cells are shown in Fig. 3(a), and clearly shows that the cell without the TRJ-buffer (cell # 1) had poorer performance among the cells with higher V_{oc} and FF, while the cell with the thickest buffer layer, 125 nm for cell # 5, had a poor tandem cell structure, with lower V_{oc} and FF.

The EQE spectra of these cells show a gradual improvement in the EQE spectra of the cells from cell #1 to cell #3, where they approach towards a matching condition for the current densities, with the highest EQE for the top sub-cell. For cell #4, this tendency reversed, and the EQE spectra of the bottom sub-cell decreased. In cell #5, the EQE and the J−V characteristic curves appear strange, probably because the cell was not performing as a tandem cell. Therefore, we consider the 75-nm-thick TRJ

buffer layer as the optimized buffer layer for the tandem solar cell. The current densities of the top cell calculated by EQE were 9.31, 9.18, 9.54, and 9.09 mA/cm^2, and the current densities of the bottom cell were 21.12, 19.49, 17.90, and 15.96 mA/cm^2. This shows that the higher efficiency of current matching in the top cell and the bottom cell, the higher efficiency of the tandem solar cell is possible. In particular, the current density is matched due to the low current density of the top cell, and thus there is a limit that shows lower efficiency than the c-Si single junction solar cell. However, if the spectral characteristics can be shifted to shorter wavelengths by applying higher bandgap material to the top cell and be got higher current densities on the top cell, the efficiency of the tandem junction solar cell can be improved.

4. Conclusions

Our results showed that the thickness of the TRJ buffer layer plays a significant role in improving the performance of the tandem solar cell. Here, the p-type nanocrystalline silicon layer was used as the buffer layer. Because of its low activation energy, the tunneling and recombination at this layer improves, as reflected in the improved device performance. We considered the thickness of this layer as closely similar to the width of the

tunnel junction, W. With a thicker barrier, the tunneling and recombination was worse than that with a thinner or even without a TRJ-buffer layer. Therefore, the 75-nm-thick buffer layer showed the best device performance.

Acknowledgments

References

1. Willemen, J.A., Zeman, M., Metselaar, J.W., "Computer modeling of amorphous silicon tandem cells," in: Anon (Ed.) Proceedings of the 24th IEEE Photovoltaic Specialists Conference. Part 2 (of 2), IEEE, Piscataway, NJ, United States, Waikoloa, HI, USA, pp. 599-602, 1994.

2. Hegedus, S.S., Kampas, F., Xi, J., "Current transport in amorphous silicon np junctions and their application as tunnel junctions in tandem solar cells," Appl. Phys. Lett., Vol. 67, NO. 6, p. 813, 1995.

3. Rath, J.K., Rubinelli, F.A., Schropp, R.E.I., "Microcrystalline n- and p-layers at the tunnel junction of a-Si:H/a-Si:H tandem cells," J. Non. Cryst. Solids, Vol. 227-230, No.2, p.1282, 1998.

4. Rath, J.K., Rubinelli, F.A., Schropp, R.E.I., "Effect of oxide treatment at the microcrystalline tunnel junction of a-Si:H/a-Si:H tandem cells," J. Non. Cryst. Solids, Vol. 266-269, No. B, pp. 1129-1133, 2000.

5. Rubinelli, F.A., Rath, J.K., Schropp, R.E.I., "Microcrystalline n-i-p tunnel junction in a-Si:H/a-Si:H tandem cells," J. Appl. Phys., Vol. 89, pp. 4010-4018, 2001.

6. Löffler, J., Gordijn, A., Stolk, R.L., Li, H., Rath, J.K., Schropp, R.E.I., "Amorphous and micromorph silicon tandem cells with high open-circuit voltage," Sol. Energ. Mater. Sol. Cells, Vol. 87, pp. 251-259, 2005.

7. Belfar, A., Mostefaoui, R., "Simulation of n1-p2 microcrystalline silicon tunnel junction with AMPS-1D in a-Si:H/μc-Si:H tandem solar cells," J. Appl. Sci., Vol. 11, pp. 2932-2939, 2011.

8. Lin, Y.S., Lien, S.Y., Wang, C.C., Hsu, C.H., Yang, C.H., Nautiyal, A., Wuu, D.S., Tsai, P.C., Lee, S.J., "Optimization of recombination layer in the tunnel junction of amorphous silicon thin-film tandem solar cells," Int. J. Photoenergy, Vol. 2011, pp. 264709 -1 - 264709 -5, 2011.

9. Chang, P.K., Lu, C.H., Yeh, C.H., Houng, M.P., "High efficiency a-Si:H/a-Si:H solar cell with a tunnel recombination junction and a n-type μc-Si:H layer," Thin Solid Films, Vol. 520, pp. 3684-3687, 2012.

10. Lee, Y., Ai, D.V., Kim, S., Han, S., Kim, H., Yi, J., "A study of tunnel recombination junction on a-Si:H/HIT tandem structure solar cell," in: 39th IEEE Photovoltaic Specialists Conference, PVSC 2013, Institute of Electrical and Electronics Engineers Inc., Tampa, FL, pp. 1361-1363, 2013.

11. Yu, B., Zhu, F., Wang, H., Li, G., Yan, D., "All-organic tunnel junctions as connecting units in tandem organic solar cell," J. Appl. Phys., Vol. 104, pp. 114503-1 – 114503-15, 2008.

12. Vukadinović, M., Smole, F., Topič, M., Krč, J., Furlan, J., "Numerical modelling of trap-assisted tunnelling mechanism in a-Si:H and μc-Si n/p structures and tandem solar cells," Sol. Energ. Mater. Sol. Cells, Vol. 66, pp. 361-367, 2001.

13. Yao, W.J., Zeng, X.B., Peng, W.B., Liu, S.Y., Xie, X.B., Wang, C., Liao, X.B., "The p recombination layer in tunnel junctions for micromorph tandem solar cells," Chin. Phys., Vol. 20, No. 7, pp. 078402-1- 078402-5, 2011.

14. Li, G.J., Hou, G.F., Han, X.Y., Yuan, Y.J., Wei, C.C., Sun, J., Zhao, Y., Geng, X.H., "The study of a new n/p tunnel recombination junction and its application in a-Si:H/μc-Si:H tandem solar cells," Chin. Phys., Vol. 18, pp. 1674-1678, 2009.

15. Chung, J.W., Ji, E.L., Ji, H.J., Jeong, C.L., Cho, J.S., Young, K.K., Yi, J., O, O.P., Song, J., Kyung, H.Y., "The properties of n-μc-SiO:H inter-layers for thin-film silicon tandem solar cells," in: 2009 34th IEEE Photovoltaic Specialists Conference, PVSC 2009, Philadelphia, PA, pp. 000759-000762, 2009.

16. Nakanishi, A., Takiguchi, Y., Miyajima, S., "Device simulation of $CH_3NH_3PbI_3$ perovskite/heterojunction crystalline silicon monolithic tandem solar cells using an n-type a-Si:H/p-type μc-Si$_{1-x}$ O$_x$:H tunnel junction," Phys. Status Solidi. A. Appl. Mater. Sci., Vol. 213, pp. 1997-2002, 2016.

17. Kateb, M.N., Tobbeche, S., Merazga, A., "Influence of μc-Si:H tunnel recombination junction on the performance of a-Si:H/μc-Si:H tandem solar cell," Optik, Vol. 139, pp. 152-165, 2017.

18. Luo, P.Q., Zhou, Z.B., Chan, K. Y., Tang, D. Y., Cui, R.Q., Dou, X.M., "Gas doping ratio effects on p-type hydrogenated nanocrystalline silicon thin films grown by hot-wire chemical vapor deposition," Appl. Surface Sci. Vol. 255, No. 5, pp. 2910-2915, 2008.

19. Schropp, R.E.I., Zeman, M., "Amorphous and Microcrystalline Silicon Solar Cells: Modeling, Materials and Device Technology," First ed. Kluwer Academy Publishers, pp. 44-45, 1998.